IPACK2022-97421

DETERMINATION OF THE THERMAL PERFORMANCE LIMITS FOR SINGLE PHASE LIQUID COOLING USING AN IMPROVED EFFECTIVENESS-NTU COLD PLATE MODEL

Alfonso Ortega Villanova University Villanova, USA

Carol Caceres Villanova University Villanova, USA

Umut Uras Villanova University Villanova, USA

Deogratius Kisitu Villanova University Villanova, USA

Uschas Chowdhury NVIDIA Corporation Santa Clara, USA

Vahideh Radmard **NVIDIA** Corporation Santa Clara, USA

Ali Heydari **NVIDIA Corporation** Santa Clara, USA

ABSTRACT

Cold plates are at the heart of pumped liquid cooling systems. In this paper, we report on combined experimental, analytical, and computational efforts to characterize and model the thermal performance of advanced cold plates in order to establish their performance limits. A novel effectiveness-NTU formulation is introduced that models the fin array as a secondary "pseudofluid" such that accurate crossflow effectiveness models can be utilized to model the cold plates using well-known formulations. Experimental measurements and conjugate CFD simulations were made on cold plates with fin and channel features of order 100 um with water-propylene glycol (PG) mixtures as coolants. We show that for a fixed fin geometry, the best thermal performance, regardless of the pressure drop, is achieved when the flow rate is high enough to approach the low NTU convective limit which occurs for NTU approaching zero. For the model cold plate evaluated in this study, the lowest thermal resistance achieved at a flow rate of 4 LPM was 0.01 C/W, and the convective limit was 0.005 C/W. However, for a fixed pressure drop, the optimal cold plate should be designed to meet its TDP at the highest possible effectiveness in which the lower limit of thermal resistance is the advective limit achieved for NTU > 7. For the tested cold plate the advective limit for the thermal resistance is 0.003 C/W, but this limit can only be achieved if it is practically feasible to increase the surface area and heat transfer coefficient to maximize NTU for a targeted TDP.

Keywords: Cold plates, Liquid cooling, Effectiveness/NTU, Heat exchanger, Analytical modeling, Cooling limits

NOMENCLATURE

Area, m² A

C	Heat Capacitance, W/°C
c_p	Specific heat, J/kg.K
H	Height, m
\overline{h}	Heat transfer coefficient, W/m ² K
L	Length, m
LMTD	Logarithmic mean temperature difference
m	Fin parameter, 1/m
m	Mass flow rate, kg/s
N	Number of fins
NTU	Number of transfer units
p	Fin Perimeter, m
P	Pressure, Pa
PG	Propylene glycol
PCM	Phase change material
R	Thermal resistance, °C/W
T	Temperature, °C
TIM	Thermal interface material
TTV	Thermal test vehicle
t	Thickness, m
V	Velocities, m/s

Greek Symbols Effectiveness

U	Lifectiveness
η	Efficiency
ρ	Density, kg/m ³
μ	Dynamic viscosity, Pa s
ΔP	Pressure drop, Pa
∇	Vector differential operator

Width, m

Subscripts

Cold Plate base b

CPCold Plate С Cross section Channel chCross-flow cfFluid f Fin fin exp Experimental Heat sink hs Maximum max Minimum min Overall 0 S Solid Single stream SS

Superscripts

in	Inlet
out	Outlet
t	Fin tip

1.0 INTRODUCTION AND BACKGROUND

Whereas thermal management of electronic computing systems using air-cooling is, for obvious reasons, the preferred approach, practically achievable thermal capacitance and heat transfer coefficients introduce cooling limits that are rapidly being surpassed in high performance computing and enterprise systems. With increasing performance, power dissipation in rack servers demand increasingly large, air-cooled heat sinks, increasingly high air-flow velocities, and increasingly large server enclosures. The practical limits of air-cooling are thus imposed by limits on acoustic noise, achievable flow rates with low-profile fans, and limits on the rack server density which ultimately translates into data center white space. Because of these limitations, indirect or direct-to-chip single phase liquid cooling using cold plates mounted directly on high power components is increasingly accepted as the next generation cooling technology.

Direct-to-chip liquid cooling utilizes a cold plate mounted directly onto server components to remove generated heat. The design of liquid cooled heat sinks or cold plates is far from new and a comprehensive review of the literature describing their analysis and design is beyond the scope of this study. The most commonly utilized and studied geometry is the straight or parallel plate fin geometry, illustrated in Figure 1. The coolant flow, typically water with additives, enters an inlet manifold, subdivides, and flows through the individual fin channels, and exits through an exit manifold. Heat is conducted through the base plate, into the fins, and is dissipated into the coolant flow.

Typical of the literature is the study of Qu and Mudawar [1] who numerically and experimentally analyzed three-dimensional fluid flow and heat transfer in rectangular microchannel water-

cooled cold plates. They studied the effect of channel Reynolds number and heat flux on cooling performance.

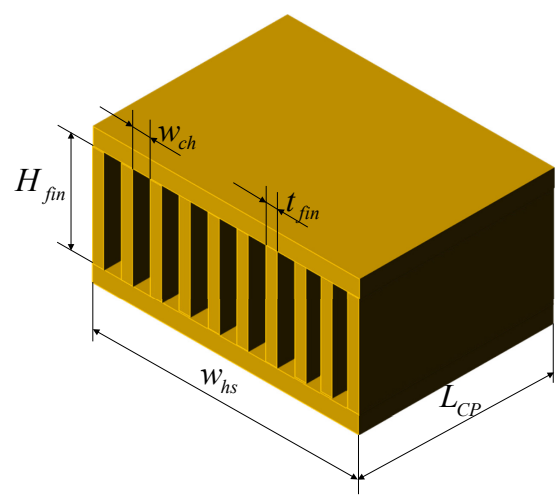


Figure 1. Nomenclature of a parallel plate fin cold plate.

The influence of flow rate and the geometric parameters such as channel dimensions, base thickness, fin thickness, and height on the cooling performance of liquid-cooled cold plates have been widely investigated [2]–[4]. Kandlikar [5] and others have classified the dimensions of the fin channels in cold plates, designating them as macro, mini and micro-channels. Micro-channels, with channel widths below 100 µm, have been extensively studied, in particular with application to micro-fabrication directly onto silicon. In a seminal study, Tuckerman et al., [6] showed that water flow through micro-channels can dissipate heat up to 790 W/cm². The literature since has been summarized by Garimella [7]. The widespread acceptance of microchannel based cooling has been deterred by practical limitations such as high pressure drop and the need for filtration to avoid clogging due to the reduced channel size.

Optimization studies [4] in which minimization of thermal resistance and pressure drop were the objectives, have generally converged on fin thickness and fin spacing of order 100-200 μm , and fin heights of order 1-2 mm (i.e. channel aspect ratios of 10 to 20) for copper cold plate fin structures. We shall refer to geometric regime as "mini-channels." These geometric dimensions coincide with easily achievable structures using the highly efficient skiving method for their manufacture. The flow distribution (single pass, split flow, parallel flow, impingement flow) and flow regime (developed or developing) also play a major role in reducing thermal resistance and increasing the heat transfer coefficient.

In this paper, the practical limits of direct to chip liquid (i.e. water) cooling are examined for removable cold plates that are externally attached to high power devices. We will show that the effectiveness-NTU theory of heat exchangers can be easily adapted for cold plates. The theory, which is validated by experimental and computational data, elucidates the limiting

physics for the thermal performance of mini-channel parallel flow cold plates.

2.0 EFFECTIVENESS-NTU MODEL FOR COLD PLATES

To design and evaluate heat exchangers, the effectiveness-NTU method developed by Kays and London [8] is widely used in industry and the scientific community. The effectiveness determines the heat exchanger limits, where the maximum or ideal performance is achieved when the effectiveness is equal to unity. However, in electronic cooling devices such as heat sinks and cold plates, the common performance metric used is thermal resistance, despite the fact that cold plates and heat sinks are in fact single-sided heat exchangers, and much can be learned from investigating their performance using this well-known theory.

For air-cooled heat sinks, Copeland [9], [10] effectiveness-NTU method assuming an isothermal heatsink. His methodology, which is reviewed in the following section, implicitly assumes that the solid side heat capacity is larger than that of the fluid. We will refer to this approach as the Single Stream approach. Deans et al. [11] developed a novel approach in which they imagine the heat flow through the solid fins as that of a "pseudo-fluid" flowing from the heat sink base temperature, i.e. the inlet temperature, to the fin tip temperature, i.e. the exit temperature as shown in Fig. 2. Thus, the heat sink can be modeled as a two-fluid cross-flow heat exchanger, with one fluid being the coolant, and the second fluid being the solid pseudofluid. We shall call this the Cross-Flow Model. Valenzuela and Ortega [12] extended the work of Deans to single and two-phase cold plates. They found that for liquid cooled cold plates, unlike air-cooled heat sinks, the fluid side capacitance may under certain circumstances exceed the solid side capacitance, thus invalidating the Single-Stream model. As will be seen, the cold plate thermal resistance may be expressed in terms of the heat exchanger effectiveness and the limits on the effectiveness can be immediately applied to find the performance limits of the cold plate.

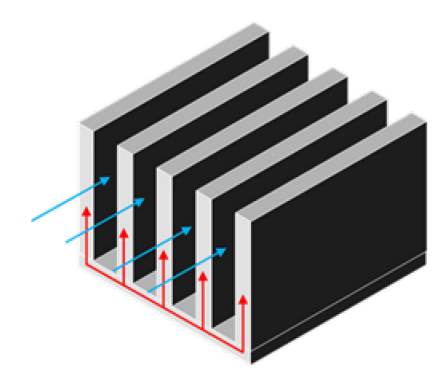


Figure 2. Cold plate modeled as a two-fluid Cross-Flow heat exchanger with liquid flow (blue) and solid pseudo-flow (red)

2.1 SINGLE STREAM HEAT EXCHANGER MODEL

The thermal resistance of a cold plate is commonly expressed as:

$$R_{CP} = \frac{T_b - T_f^{in}}{\dot{Q}} = \frac{T_b - T_f^{in}}{\dot{m}c_p(T_f^{out} - T_f^{in})}$$
(1)

Furthermore, from the theory of heat exchangers, the effectiveness is defined as

$$\varepsilon = \frac{\dot{Q}}{\dot{Q}_{\text{max}}} = \frac{\dot{Q}}{C_{\text{min}}(T_b - T_f^{in})} = \frac{C_{\text{min}}(T_f^{out} - T_f^{in})}{C_{\text{min}}(T_b - T_f^{in})} \tag{2}$$

from which it can be readily seen that

$$R_{CP} = \frac{1}{\dot{m}c_{p}\varepsilon} \tag{3}$$

For the case of $C_{\rm max}$ / $C_{\rm min}$ \rightarrow ∞ , i.e. when one capacitance is much larger than the other, as in the present case with the solid capacitance much larger than the fluid, the ϵ -NTU relationship is given by [8]

$$\varepsilon = 1 - e^{-NTU} \tag{4}$$

and thus

$$R_{CP} = \frac{1}{\dot{m}c_{n}(1 - e^{-NTU})}$$
 (5)

Since the theory assumes that the solid side is isothermal because of its infinite capacitance, and since the cold plate fins are not isothermal, it is common to correct this defect by the overall surface efficiency, η_o . The NTU for the single sided-fin heat exchanger is thus defined as:

$$NTU = \frac{\eta_o \bar{h} A_s}{\dot{m} c_p} \tag{6}$$

In Eq. (6), the heat transfer coefficient \overline{h} is the surface averaged heat transfer coefficient, where the local heat transfer coefficient h in the channel is defined in terms of the local mixed mean temperature

$$h = \frac{\dot{q}}{(T_s - T_f)} \tag{7}$$

Large NTU Limit

From Eq. (5), it is seen that for NTU > 7, $\varepsilon \to 1$, i.e. the effectiveness approaches its maximum of 1.0. In this limit the cold plate resistance approaches

$$R_{CP} = \frac{1}{\dot{m}c_p} \tag{8}$$

This is the thermodynamic or advective limit for the thermal resistance, achieved when the convective resistance $(1/\eta_o \bar{h} A_s) \rightarrow 0$. For a given mass flow rate, the thermal resistance cannot be lower than this limit, but it can only be reached if $\eta_o \bar{h} A_s$ is sufficiently high to guarantee *NTU* greater than about 7. Equation (3) can alternatively be expressed as

$$\frac{R_{CP}}{R_{CP,\min}} = \frac{1}{\varepsilon} \tag{9}$$

Small NTU Limit

In Eqn. (5) we can expand the exponential term in a Maclaurin series thusly:

$$1 - e^{-NTU} = 1 - \left[\frac{\left(-NTU \right)^{0}}{0!} + \frac{\left(-NTU \right)^{1}}{1!} + \frac{\left(-NTU \right)^{2}}{2!} + \frac{\left(-NTU \right)^{3}}{3!} + \dots \right]$$
(10)

For small NTU

$$1 - e^{-NTU} \to NTU \tag{11}$$

and the resistance from Eq. (5) is given by:

$$R_{CP} = \frac{1}{\dot{m}c_{p} \left[\frac{\eta_{o}\bar{h}A_{s}}{\dot{m}c_{p}}\right]} = \frac{1}{\eta_{o}\bar{h}A_{s}}$$
(12)

This is the convective limit for the cold plate thermal resistance. For a fixed fin geometry, the cold plate resistance will be limited to this lower value as mass flow rate is increased because the increase in mass flow rate cannot be balanced by a similar increase in the heat transfer coefficient. Hence for a fixed geometry, as mass flow rate increases *NTU* will decrease, driving the thermal resistance to the convective limit, Eq. (12).

2.2 TWO STREAM HEAT EXCHANGER MODEL

Deans et al. [11] introduced the novel concept of modeling an air-cooled heat sink as though it has two flow streams. The heat conduction path through the heat sink base and the fins is modeled as an equivalent hot fluid stream, as illustrated in Fig. 2. Following this approach, the cold plate can be modeled as a two-stream cross-flow heat exchanger using the appropriate effectiveness-NTU model for this configuration [8]. Valenzuela and Ortega [12] extended this approach to single and two-phase

liquid cooled cold plates and demonstrated excellent agreement with reported literature data.

In the two-stream model the equivalent hot flow stream is postulated to flow from the high temperature at the fin base, T_b , to the low temperature at the fin tip, T_{fin}^t . Based on this assumption, the heat transport by the hot stream is

$$\dot{Q} = C_s (T_b - T_{fin}^t) \tag{13}$$

The effectiveness is defined as,

$$\varepsilon = \frac{\dot{Q}}{\dot{Q}_{\text{max}}} = \frac{\dot{Q}}{C_{\text{min}}(T_b - T_f^{in})}$$
(14)

Here C_{min} is the minimum flow capacitance. Valenzuela and Ortega [12] have shown that for liquid cooled cold plates, C_{min} can be either the fluid or the solid capacitance. Effectiveness definition (14) shows that the minimum temperature is given by the fluid at the inlet of the cold plate. Using traditional thin plate fin theory with an adiabatic tip boundary condition, the equivalent solid side heat capacitance can be derived as:

$$C_s = \frac{N\overline{h}P}{m} \frac{\tanh(mH_{fin})}{1 - \frac{1}{\cosh(mH_{fin})}}$$
(15)

where the traditional fin parameter m is given by $m = \sqrt{\frac{\overline{h}P}{kA_c}}$.

The effectiveness can be defined using either the solid or the fluid side capacitance:

$$\varepsilon = \frac{C_s(T_b - T_t)}{C_{\min}(T_b - T_f^{in})} = \frac{C_f(T_f^{out} - T_f^{in})}{C_{\min}(T_b - T_f^{in})}$$
(16)

Valenzuela and Ortega recommended using the effectiveness expression for cross-flow heat exchangers with both fluids mixed which is given by [8].

$$\varepsilon_{cf} = \frac{NTU}{\frac{NTU}{1 - e^{-NTU}} + \frac{C^*NTU}{1 - e^{-C^*NTU}} - 1}$$
(17)

where,

$$C^* = \frac{C_{\min}}{C_{\max}} = \frac{\min(\dot{m}c_p, C_s)}{\max(\dot{m}c_p, C_s)}$$
(18)

3.0 EXPERIMENTAL AND COMPUTATIONAL OBSERVATIONS OF LIMITING BEHAVIOR

3.1 Cold Plate

In order to examine the correctness of the derived one and twostream heat exchanger models of cold plates, experimental measurements were made on a modern high performance copper cold plate with skived mini-channel fins. The fin geometry and the overall cold plate dimensions are as follows in table 1:

Table 1. Cold Plate heat sink dimensions

Table 1: Cold 1 late fleat cliff difficiencies		
0.2 mm		
4 mm		
0.2 mm		
43 mm		

The flow configuration is a traditional side-in, side-out configuration with all fin channels sharing a common inlet and exit manifold. A 3D illustration of the tested cold plate is shown in Fig. 3.

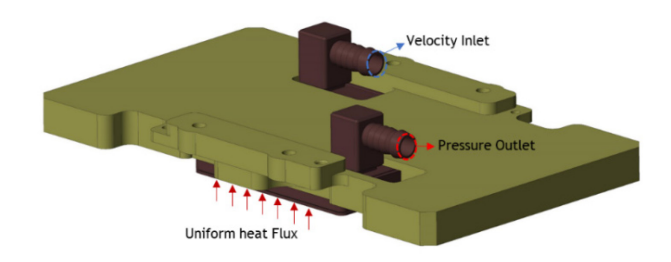


FIGURE 3: Cold Plate Geometry. CFD Simulations.

3.2 Description of experimental apparatus and measurements

The single-phase cold plate characterization rig, illustrated in Figure 4, was designed to precisely control and measure the cold plate inlet and outlet conditions. Propylene Glycol - 25% solution (PG-25) is used as the working fluid. Upstream of the cold plate is a brazed plate heat exchanger, which rejects heat from the coolant to a chilled water stream provided by a NESLAB™ HX Series recirculating chiller. The coolant is delivered to the reservoir and then to a coil heat exchanger immersed in a ThermoNESLAB isothermal bath. The bath conditions the coolant inlet temperature to the desired temperature entering the cold plate. Flow is pumped by a positive displacement gear pump controlled by a digital DC speed controller. It is then filtered and then measured by an IFM SM6004 electromagnetic flowmeter (accuracy 2% of reading).

The cold plate inlet and outlet coolant temperatures and pressures were measured using inline OMEGATM 1/8 in type-K thermocouple probes and Keyence GP-M010 (-0.1 - 1MPa) pressure sensors, respectively. The cold plate base temperature was obtained from averaging the temperatures measured with three butt-welded OMEGATM type-K thermocouples embedded in the base plate. The cold plate was mounted onto a thermal test vehicle (TTV) consisting of a copper block with a metal film heater adhered to its underside. The block was mounted in a custom, 3D printed substrate. The cold plate was fastened onto the substrate with four spring-loaded bolts, which provided a uniform loading of about 30 psi. A phase change TIM (Honeywell PTM 7950) was used to provide thermal contact between the cold plate base and the heated block. The TTV was powered by a KEYSIGHT N8762A DC power supply unit. All thermocouples were terminated in a zone box which was referenced to an ice bath.

For all experimental cases, the inlet temperature was 32 C. The volumetric flow rate was varied from 0.5 to 2.5 LPM and the heater power was fixed at 1 KW.

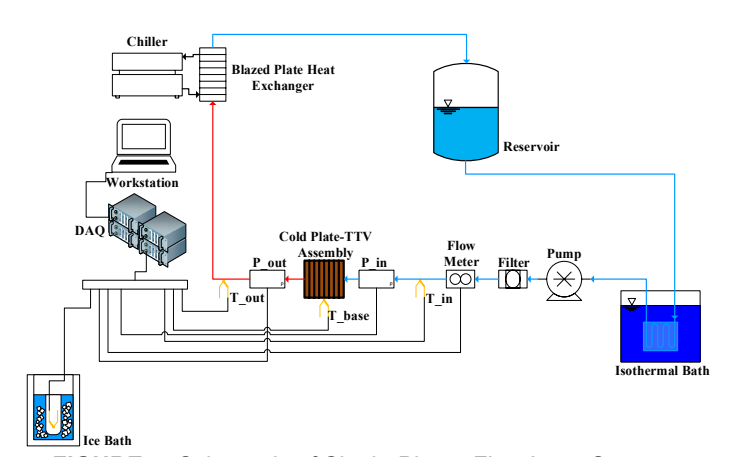


FIGURE 4: Schematic of Single-Phase Flow Loop Setup.

3.3 Experimental Effectiveness and NTU

The effectiveness is obtained from experimental data with Eq. (19).

$$\varepsilon_{\text{exp}} = \frac{\dot{m}c_p \left(T_f^{\text{out}} - T_f^{\text{in}} \right)}{C_{\text{min}} \left(T_b - T_f^{\text{in}} \right)} \tag{19}$$

Experiments were performed in a range where the fluid has the minimum heat capacitance. Therefore

$$\varepsilon_{\rm exp} = \frac{T_f^{out} - T_f^{in}}{T_b - T_f^{in}} \tag{20}$$

NTU for the measured data was also obtained experimentally. The surface averaged heat transfer coefficient was extracted from experimental data and the well-known relationship for heat transfer from isothermal channels:

$$\dot{Q} = \overline{h} A_s \eta_o LMTD \tag{21}$$

Where the overall surface efficiency is given by

$$\eta_o = 1 - \frac{NA_{fin}}{A_s} (1 - \eta_{fin})$$
 (22)

and the fin efficiency by

$$\eta_{fin} = \frac{\tanh(mH_{fin})}{mH_{fin}} \tag{23}$$

$$m = \sqrt{\frac{\overline{hp}}{kA_c}} \tag{24}$$

The log mean temperature difference is computed as

$$LMTD = \frac{(T_b - T_f^{in}) - (T_b - T_f^{out})}{\ln\left(\frac{T_b - T_f^{in}}{T_b - T_f^{out}}\right)}$$
(25)

Equations (21-25) are solved using a non-linear root solver to compute the heat transfer coefficient. Finally, the experimental NTU is obtained with eqn. (26)

$$NTU_{\rm exp} = \frac{\eta_o \overline{h} A_s}{C_{min}}$$
 (26)

4.0 Description of CFD modeling

4.1 Basic Assumptions

The following assumptions are applied to the governing equations of mass, momentum, and energy:

- The flow is incompressible, three-dimensional and in a steady state
- Fully laminar flow in all channels (Re<200)
- Radiation and viscous heat generation are negligence
- Gravity effect is included
- Temperature effect on the thermophysical properties of the coolant is considered

4.2 Governing Equations

The governing equations for a 3-D conduction-convection heat transfer problem in an incompressible, steady laminar flow regime are as follows:

Continuity equation:

$$\nabla \cdot \vec{V} = 0 \tag{27}$$

Where, V is velocity vector field.

Navier-Stokes equation:

$$\rho_f(\vec{V} \cdot \nabla)\vec{V} = -\nabla P + \mu_f \nabla^2 \vec{V} \tag{28}$$

Where, ρ_f is the density of the fluid, P represents the pressure field, and μ_f is the coolant absolute viscosity.

Energy equation of solid phases:

$$\nabla^2 T_{\rm s} = 0 \tag{29}$$

In which ^S represents solid phase.

Energy equation of the liquid phase:

$$\rho_f c_p(\vec{V} \cdot \nabla) T_f = k_f \nabla^2 T_f \tag{30}$$

Where, c_p stands for the specific heat capacity of the fluid, and k_f denotes fluid conductivity.

4.2 Numerical Domain and Boundary Conditions

The coolant enters the inlet port through the "velocity inlet" and returns from the "pressure outlet" port placed on the top of the cold plate. Adiabatic and no-slip boundary conditions are imposed at the interfaces between the fluid and liquid, the side walls, and the plastic cover. The lateral surfaces of the fins and the surfaces which are in touch with coolant are thermally coupled.

4.3 Numerical Approach

6SigmaET [13] software is used to perform the fluid dynamics and heat transfer modeling of the cooling system. The software uses the finite volume method (FVM) to discretize the governing equations of continuity, Navier-Stokes, and energy equations in the computational domain on a staggered grid. The field functions of velocity, pressure, and temperature are calculated through iterative SIMPLE algorithm. The differential equations are discretized through a hierarchy of cartesian grids and a faceto-cell connectivity graph. 6SigmaET uses multi-level unstructured solver to accurately capture the pressure drop and heat transfer in the model. The method provides accuracy as the structured griding while is more flexible in resolving arbitrary geometries and different solution scales. Grid sensitivity analysis is done based on both case thermal resistance and cold plate's pressure drop. Increasing the number of grids to more than 25 million results in less than 3% variation in the thermal resistance

and pressure drop values, respectively. Accordingly, 26 million grids assure the mesh independence of the CFD results.

5.0 RESULTS AND DISCUSSION

Figure 5 shows the experimentally measured cold plate thermal resistance and pressure drop for a water/PG-25 mixture for flow rates up to 2.6 LPM. The minimum thermal resistance is 0.012 °C/W obtained at the highest flow rate. As commonly observed, the highest pressure drop of 6.3 psi is found at the highest flow rate. It is observed that the thermal resistance decreases monotonically with flow rate, but the rate of decrease with flow rate decreases. By observing the data framed against the limiting trends discussed in the previous section, it becomes clear that the thermal resistance approaches a limit at increasing flow rate, although that limit has not been reached in the experimental data shown in the figure.

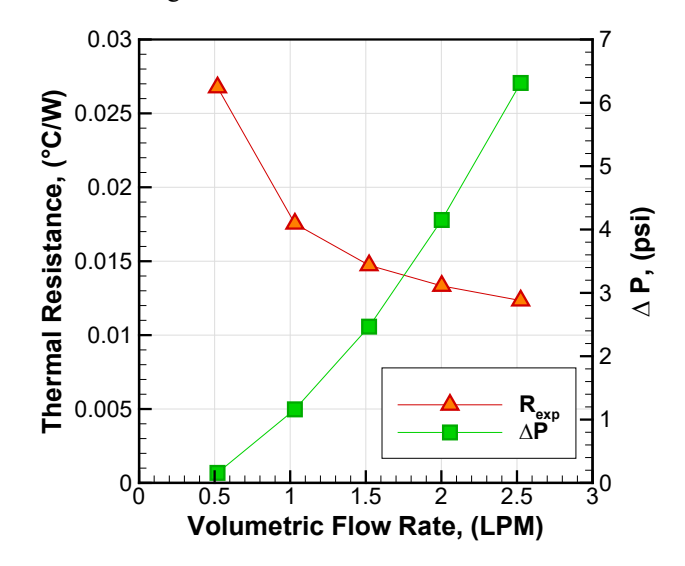


FIGURE 5: Experimental Cold Plate Thermal Resistance and Pressure Drop.

In order to extend the experimental data, Figure 6 compares the measured experimental data to the CFD calculations and to the Single Stream and Cross-Flow effectiveness models derived in the previous section. The comparison shown in Fig. 6 reveals that results obtained by crossflow heat exchanger ε-NTU model show the best agreement with the experimental data. The minimum and maximum difference between the crossflow model and experimental results are calculated as 0.9 % at 2.5 LPM and 22.7% at 0.5 LPM, respectively. The reason for the discrepancy between the experiments and the crossflow model at the lowest flow rate of 0.5 LPM may be caused by the effects of upstream heat conduction into the inlet manifold which pre-heats the coolant before it enters the fin channels. The Single-stream heat exchanger model results show good agreement with experimental results with increasing discrepancy at higher flow rates. The computational results follow a similar trend as the Cross-Flow model results. This may account for the discrepancy

between the two approaches. The blue line in Figure 6 is the thermal resistance computed from the low NTU convective limit model. It is observed that both of the effectiveness-NTU models and the computational results show asymptotic trends toward the convective limit of about 0.006 C/W. The measured data and best models predict a thermal resistance of 0.01 C/W at 4 LPM.

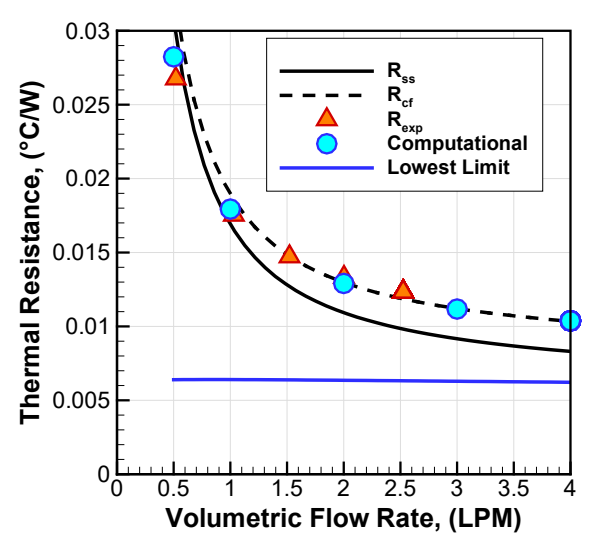


FIGURE 6: Thermal Resistance Comparison.

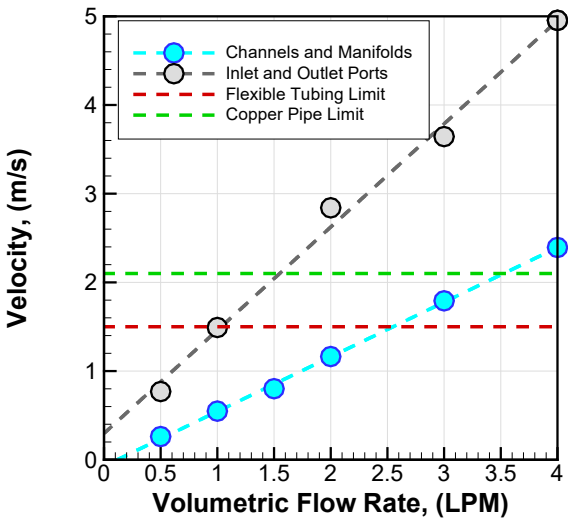


FIGURE 7: Maximum Allowable Cold Plate Velocities (CFD Results) Compared to Erosion Limits.

The minimum thermal resistance that can be achieved for a given cold plate is theoretically the convective limit for increasingly high mass flow rates. However, the maximum flow rate is also constrained by the potential mechanical damage by erosion that can be caused by elevated velocities. The ASHRAE liquid cooling guidelines [14] were used in order to calculate the allowable flow rates for the candidate cold plate. Results are shown in Fig. 7 in which velocities computed from the simulations were compared to the allowable velocities as dictated by the standard. It is shown that the velocity limits from

1.5 to 2.1 m/s are exceeded at a flow rate of 3.5 LPM, hence, for the candidate cold plate, erosion limits would prohibit achieving the theoretical lower limit for thermal performance.

Figure 8 presents the data of Fig. 6 in terms of the unit thermal resistance which is useful for comparing the performance of the given fin geometry regardless of the actual size of the total finned or heated area of the cold plate. It is seen that the asymptotic low NTU limit is about 0.17 °C-cm²/W and the lowest predicted resistance at 4 LPM for this cold plate is 0.25 °C-cm²/W.

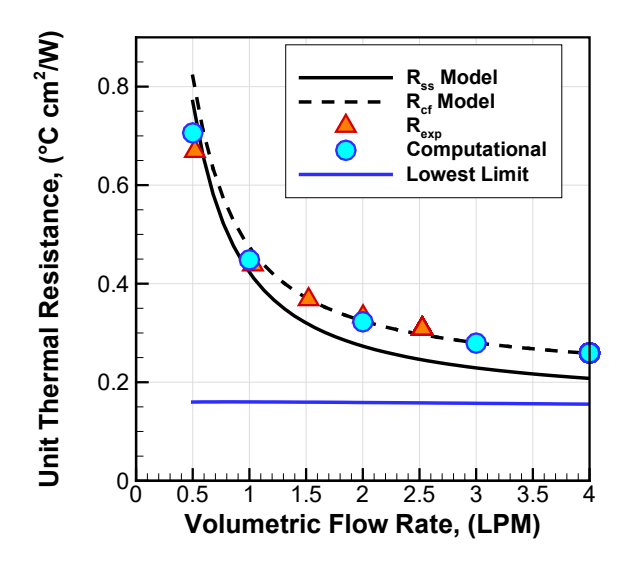


FIGURE 8: Unit Thermal Resistance Comparison.

The companion computational study can be used to further examine the cold plate thermal behavior. Whereas the experimental constraints allowed only a small, finite temperature measurements at the base, the computational model allowed an examination of the continuous temperature profile at the cold plate base. Figures 9 shows the temperature distribution of the cold plate base at 0.5 and 1 LPM, where flow is from left to right. The maximum predicted temperature was 74.8 °C at 0.5 LPM and 61.3 °C at 1 LPM.

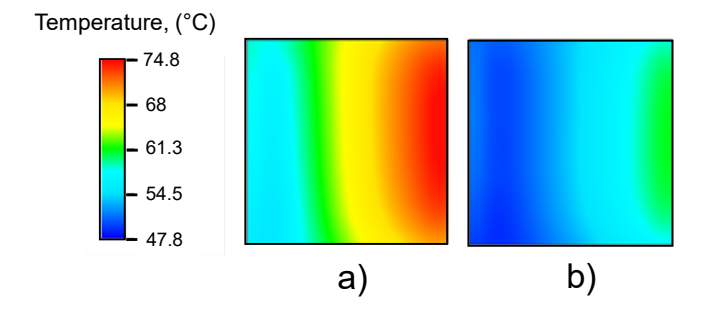


FIGURE 9: Temperature distribution over the cold plate base at (a) 0.5 LPM and (b)1 LPM.

As the flow rate is increased up to 4 LPM, the temperature distribution at the spanwise centerline of the base reveals

artifacts that are a product of the cold plate design. In the inlet region it can be observed that the temperature surprisingly decreases and then increases linearly further downstream. This is readily explained by strong axial heat conduction into the inlet manifold that has the effect of pre-heating the fluid before it enters the finned section. When the flow enters the finned section, starting at x=0 in Figure 10, the fins transport heat upwards, i.e. away from the base, hence causing the base temperature to initially decrease. In the finned section, the temperatures increase linearly indicating that the flow rapidly achieves a thermally and hydrodynamically fully-developed state. Furthermore, the linear increase also indicates that the finned section responds as though it is exposed to a uniform base heat flux condition, rather than an isothermal condition. At the exit, the temperature profile does not indicate strong axial heat conduction evidently because the flow exiting is at elevated temperature, hence the exit manifold is also heated and hence does not promote axial conduction.

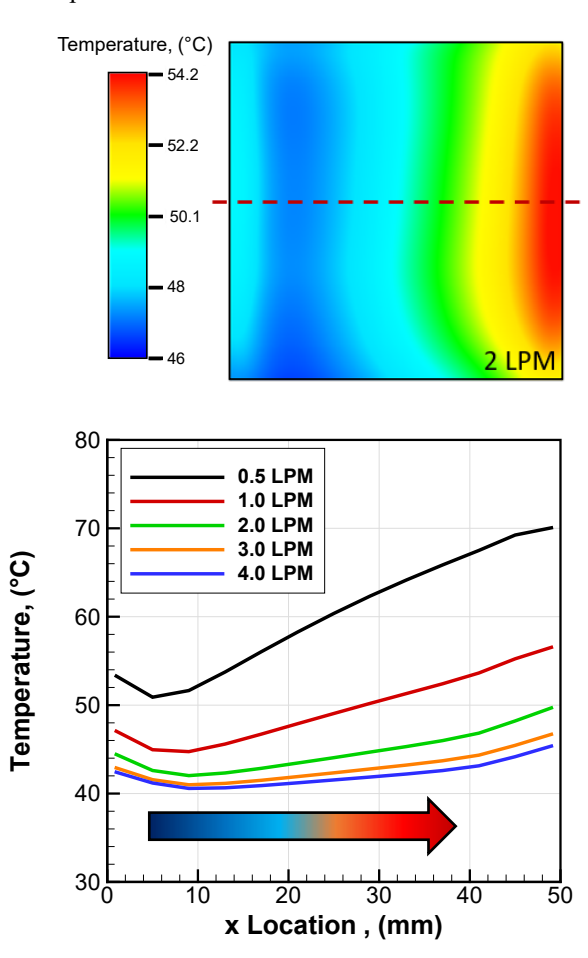


FIGURE 10: Temperature distribution along a center line at the cold plate base for different flow rates.

The importance of the heat exchanger effectiveness on the performance of cold plates has been previously discussed and Fig. 11 shows the measured and predicted effectiveness of the test cold plate with respect to volumetric flow rate. The experimentally measured effectiveness agrees reasonably well with the cross-flow model but not as well as with the single-stream model. The error of the crossflow model for flow rate from 0.5 LPM to 2.5 LPM relative to experimental results is between 5.8% and 18.9%. On the other hand, the error of the single stream model for flow rate from 0.5 LPM to 2.5 LPM relative to experimental results is between 0.7% and 46.5%, respectively. The data and models illustrate that for a fixed cold plate geometry, the effectiveness is highest at low flow rates and drops monotonically with increasing flow rate.

Based on the experimental data, the effectiveness of the cold plate is between 0.99 and 0.46 for the specified volumetric flow rate range. As seen in Fig. 6, the thermal resistance also decreases with increasing flow rate. If one considers the cold plate effectiveness as a measure of the efficient use of the coolant flow rate, it is then readily seen that for efficient use of the flow, the exiting flow temperature should be driven as high as possible, with a maximum being the cold plate metal temperature. Thus, an efficiently performing cold plate should meet its thermal design point while operating at a high effectiveness.

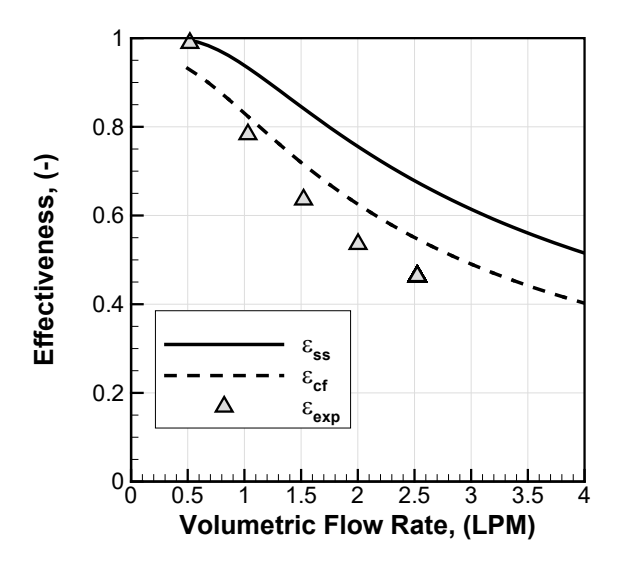


FIGURE 11: Cold Effectiveness Comparison between Experiments Single and Two Streams Model.

This point is well illustrated if one looks at the thermal resistance and effectiveness when plotted against NTU, as in Figure 12. In this presentation the experimental data at the lowest flow rate have the highest NTU and the highest flow rates have the lowest NTU. Thus, with increasing flow rate, the behavior moves from the right to the left. At the lowest flow rates, the effectiveness is highest because the residence time of the fluid within the channels is at its highest, hence the exiting fluid temperature is

high. Here it is seen that the lowest thermal resistance was achieved at effectiveness of 0.45. If for example the TDP called for a design thermal resistance of 0.01 C/W, a more efficient design would deliver the design thermal resistance at an NTU of 4 or 5, which would require less mass flow and less pressure drop. That design would require a greater fin surface area and higher heat transfer coefficient. Both can be achieved by decreasing the fin pitch and increasing the fin height.

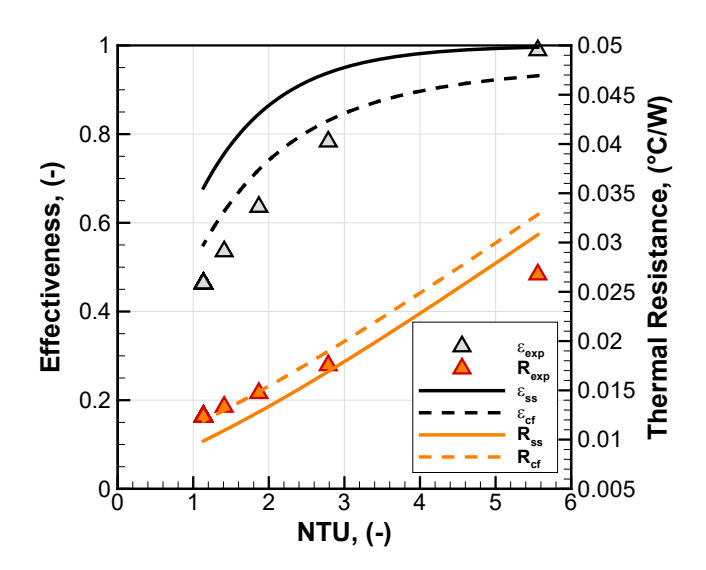


FIGURE 12: Effectiveness and Thermal Resistance Behavior for Different NTUs.

Figure 13 shows the experimental data and the cross-flow model simulation for thermal resistance plotted against flow capacitance. Here the experimental data have a relatively narrow span, but the model data shown in red extend the span from very low flow rates to very high flow rates, well beyond the 2.5 LPM of the experimental data. It is observed that at the lowest flow rates, the experimental data and the model both approach the large NTU limit, $R_{NTU\to\infty} = 1/\dot{m}c_n$. The high NTUs are easily achieved because of the low mass flow rate. At the highest flow rates, the experimental data have a low NTU of about 1.0. The model indicated by the red line shows that at elevated flow rates leading to increasingly low NTU, the thermal resistance approaches the low NTU limiting behavior. It is interesting to note that the low NTU limit, $R_{NTU\to 0} = 1/\eta_o \bar{h}A$, does not reach an asymptotically constant value of the thermal resistance at increasing flow rates. The reason for this is that the surface averaged heat transfer coefficient slowly increases with increasing flow rate as a result of the increasing thermal and hydraulic entry length with flow rate. This slow increase in the heat transfer coefficient is manifested in the slow drop in the thermal resistance.

The graphical results of Figs. 6 and 13 indicate that for the cold plate tested, which is representative of well-designed skived copper cold plates, the resistance at 4 LPM was about 0.01 °C/W

(0.26 °C-cm²/W). The convective limit at this flow rate was 0.005 °C/W. The lowest limit, the advective limit, was 0.003 °C/W. The advective limit cannot be achieved by increasing the flow rate for the given fin geometry. It can only be achieved by re-designing the fin geometry to achieve high NTU for practical coolant flow rates.

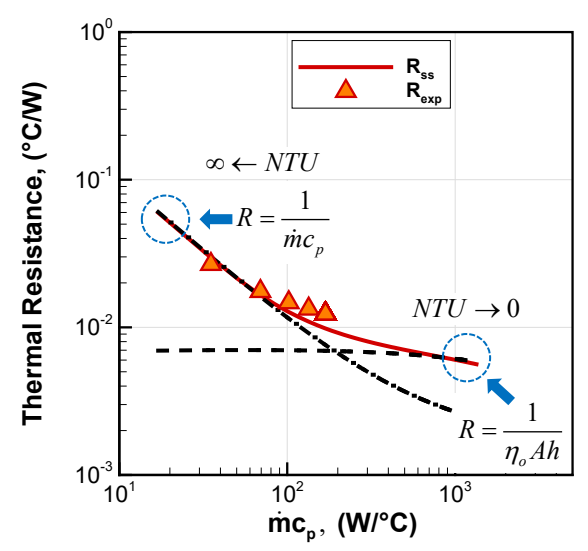


FIGURE 13: Cold Plate Theoretical Cooling Limits and Experimental Data Validation.

6. CONCLUSIONS

- Experimental measurements on an advanced straight fin mini-channel cold plate with PG-25 coolant showed good agreement with a newly formulated thermal resistance model based on a two stream Cross-Flow effectiveness-NTU model adapted for application to cold plates.
- 2. The traditional Single Stream effectiveness-NTU model adequately predicted the cold plate thermal resistance with increasing discrepancy at high flow rates.
- 3. Analysis of the model reveals two asymptotic limits: (i.e.) a low NTU convective limit in which the effectiveness approaches zero and the thermal resistance is dominated by the overall fin convective resistance, and (ii.) a high NTU limit in which the effectiveness approaches 1.0 and the thermal resistance approaches its thermodynamic or advective limit.
- 4. For a fixed cold plate fin geometry, the thermal resistance decreases monotonically with increasing mass flow rate and approaches the low NTU convective limit. For the cold plate evaluated in the present study, the convectively limited thermal resistance was 0.006 °C/W with a unit thermal resistance of 0.16 °C-cm²/W. At 4 LPM, the test cold plate achieved its lowest thermal resistance of 0.01 °C/W, indicating that even higher flow rates are necessary to achieve its theoretical convective limit. This limit is the

- practical design limit when maximum pressure drop is not a consideration in a design.
- 5. It is shown that the lowest theoretical limit for the thermal resistance is the high NTU advective limit, achieved when the cold plate effectiveness approaches a value of 1.0. This limit is achieved for NTU greater than 7. For a fixed maximum tolerable pressure drop, cold plate design should drive towards this limit by optimizing the fin geometry to maximize the NTU and thus its effectiveness while achieving the design thermal resistance.

REFERENCES

- [1] W. Qu and I. Mudawar, "Experimental and numerical study of pressure drop and heat transfer in a single-phase microchannel heat sink," *International Journal of Heat and Mass Transfer*, vol. 45, no. 12, pp. 2549–2565, Jun. 2002, doi: 10.1016/S0017-9310(01)00337-4.
- [2] X.-H. Yang, S.-C. Tan, Y.-J. Ding, and J. Liu, "Flow and thermal modeling and optimization of micro/mini-channel heat sink," *Applied Thermal Engineering*, vol. 117, pp. 289–296, May 2017, doi: 10.1016/j.applthermaleng.2016.12.089.
- [3] X. L. Xie, Z. J. Liu, Y. L. He, and W. Q. Tao, "Numerical study of laminar heat transfer and pressure drop characteristics in a water-cooled minichannel heat sink," *Applied Thermal Engineering*, vol. 29, no. 1, pp. 64–74, Jan. 2009, doi: 10.1016/j.applthermaleng.2008.02.002.
- [4] Y. Hadad *et al.*, "Performance Analysis and Shape Optimization of an Impingement Microchannel Cold Plate," *IEEE Trans. Compon., Packag. Manufact. Technol.*, vol. 10, no. 8, pp. 1304–1319, Aug. 2020, doi: 10.1109/TCPMT.2020.3005824.
- [5] S. G. Kandlikar and W. J. Grande, "Evaluation of Single Phase Flow in Microchannels for High Heat Flux Chip Cooling—Thermohydraulic Performance Enhancement and Fabrication Technology," *Heat Transfer Engineering*, vol. 25, no. 8, pp. 5–16, Dec. 2004, doi: 10.1080/01457630490519772.
- [6] D. B. Tuckerman et al., "Microchannel Heat Transfer: Early History, Commercial Applications, and Emerging Opportunities," in ASME 2011 9th International Conference on Nanochannels, Microchannels, and Minichannels, Volume 2, Edmonton, Alberta, Canada, Jan. 2011, pp. 739– 756. doi: 10.1115/ICNMM2011-58308.
- [7] S. V. Garimella and V. Singhal, "Single-Phase Flow and Heat Transport in Microchannel Heat Sinks," in 1st International Conference on Microchannels and Minichannels, Rochester, New York, USA, Jan. 2003, pp. 159–169. doi: 10.1115/ICMM2003-1018.
- [8] W. M. Kays and A. L. London, Compact heat exchangers, Repr. ed. 1998 with corrections. Malabar, Fla: Krieger Pub. Co, 1998.

- [9] D. W. Copeland, "Fundamental Performance Limits of Heatsinks," *Journal of Electronic Packaging*, vol. 125, no. 2, pp. 221–225, Jun. 2003, doi: 10.1115/1.1569262.
- [10] D. Copeland, "Optimization of parallel plate heatsinks for forced convection," in Sixteenth Annual IEEE Semiconductor Thermal Measurement and Management Symposium (Cat. No.00CH37068), San Jose, CA, USA, 2000, pp. 266–272. doi: 10.1109/STHERM.2000.837093.
- [11] J. Deans, J. Neale, W. Dempster, and C. K. Lee, "The Use of Effectiveness Concepts to Calculate the Thermal Resistance of Parallel Plate Heat Sinks," *Heat Transfer Engineering*, vol. 27, no. 5, pp. 56–67, Jun. 2006, doi: 10.1080/01457630600560643.
- [12] F. Valenzuela and A. Ortega, "A Novel Heat Exchanger Effectiveness Approach for Exploring Performance Limits of Two-Phase Mini-Channel Boilers," in 2020 19th IEEE Intersociety Conference on Thermal and Thermomechanical Phenomena in Electronic Systems (ITherm), Orlando, FL, USA, Jul. 2020, pp. 1413–1423. doi: 10.1109/ITherm45881.2020.9190481.
- [13] Future Facilities, 6SigmaET.
- [14] American Society of Heating, Refrigerating and Air-Conditioning Engineers, Ed., *Liquid cooling guidelines for datacom equipment centers*, Second edition. Atlanta, [GA]: ASHRAE, 2014.